Journal of
Materials Chemistry A

Accepted Manuscript

This is an *Accepted Manuscript*, which has been through the RSC Publishing peer review process and has been accepted for publication.

Accepted Manuscripts are published online shortly after acceptance, which is prior to technical editing, formatting and proof reading. This free service from RSC Publishing allows authors to make their results available to the community, in citable form, before publication of the edited article. This *Accepted Manuscript* will be replaced by the edited and formatted *Advance Article* as soon as this is available.

To cite this manuscript please use its permanent Digital Object Identifier (DOI®), which is identical for all formats of publication.

More information about *Accepted Manuscripts* can be found in the **Information for Authors**.

Please note that technical editing may introduce minor changes to the text and/or graphics contained in the manuscript submitted by the author(s) which may alter content, and that the standard **Terms & Conditions** and the **ethical guidelines** that apply to the journal are still applicable. In no event shall the RSC be held responsible for any errors or omissions in these *Accepted Manuscript* manuscripts or any consequences arising from the use of any information contained in them.

Cite this: DOI: 10.1039/c0xx00000x

www.rsc.org/xxxxxx

ARTICLE TYPE

Hierarchically Porous Graphene Sheets and Graphitic Carbon Nitride Intercalated Composites for Enhanced Oxygen Reduction Reaction

Kaipei Qiu*[a] and Zheng Xiao Guo[a]

Received (in XXX, XXX) Xth XXXXXXXXX 20XX, Accepted Xth XXXXXXXXX 20XX

DOI: 10.1039/b000000x

The electrocatalytic activity of graphitic carbon nitride (GCN), a potential metal-free alternative to the conventional platinum-based catalysts for oxygen reduction reaction (ORR), is restricted by its poor electrical conductivity. Introducing conductive carbon substrates can enhance the ORR performance of GCN, but until now, none of the carbon-supported GCN catalysts show both excellent catalysis selectivity and fast ORR kinetics. Two-dimensional graphene sheets (GS) may serve as a suitable substrate for GCN due to its fast electron collection and transport properties, and the structural similarity to GCN as well. In this work, we present a facile method of producing intercalated GS/GCN composites with hierarchical porosity, which is experimentally achieved for the first time. The ORR activity is optimised by tuning the amount of active sites, electrical conductivity and mass transport. The obtained material possesses 100% catalysis selectivity towards four-electron pathway, and its ORR activities outperform any other existing GCN-based catalysts. It also shows significantly improved tolerance against methanol and enhanced long-term stability, compared with the commercial platinum-loaded carbon catalyst. Thus it is expected that the hierarchically porous GS/GCN intercalated composite is a promising future ORR catalyst.

Introduction

The electrochemical performance of fuel cells and metal-air batteries depend greatly on the cathodic oxygen reduction reaction (ORR).[1] Although conventional platinum-loaded carbon composites (Pt/C) have long been regarded as effective electrocatalysts for ORR, the large-scale practical application has been hampered by the prohibitive cost of Pt, as well as its limited reserve in nature.[2] In addition Pt/C suffers from the weak long-term durability,[2b] methanol fuel crossover effect,[3] and rapid degradation against carbon monoxide impurity.[2a] Therefore finding low-cost, efficient and stable alternatives is essential to mass market the above two technologies. Over the past years, two main approaches have been taken to partly/completely replace Pt catalysts through the formation of Pt-based alloys[2c,4] or non-precious metal compounds,[5] but until now neither approach has fully met the requirements for commercialization. Very recently metal-free materials, such as nitrogen-doped carbon and its derivatives, have attracted considerable interests as the next generation ORR electrocatalysts, due to their comparable catalytic activity, reduced cost and improved durability, compared with the existing counterparts.[6]

It is commonly accepted that introducing nitrogen into a carbon matrix is a key step to synthesize highly active metal-free ORR catalysts.[6b] Despite the controversy on the exact role of nitrogen heteroatom in ORR, both quantum mechanical calculations[7] and experimental observations[8] reveal that incorporation of nitrogen, especially the pyridinic or/and graphitic species, induces a positive charge on the adjacent carbon, which can facilitate oxygen adsorption and subsequently weaken the O-O bond in the adsorbed oxygen molecules. In this regard, graphitic carbon nitride (GCN) – stacked two dimensional (2D) heptazine (C_6N_7) sheets connected by tertiary amines – may serve as a promising metal-free ORR catalyst owing to its high nitrogen content (60.9 wt% in theory and mainly of pyridinic/graphitic nature) and stable molecule structure.[9]

Unfortunately, the electrocatalytic activity of pristine GCN is restricted by its semi-conductive nature ($<10^{-2}$ S/cm), which obstructs electron transfer during the ORR process.[10] Thus introducing electron-conductive carbon materials as substrates should be a general strategy to improve the ORR performance of GCN. First-principle studies on the ORR capability of GCN have shown that if sufficient electrons are available in the GCN-O_2 system, the ORR could occur via a direct four-electron ($4e^-$) pathway, rather than the two-step two-electron ($2e^-$) pathway for the pristine GCN.[11] The first experimental attempt of carbon-supported GCN composites was to mechanically blend GCN with carbon black (CB).[12] The GCB/CB composites showed much improved onset potential and reduction current density, compared with pristine GCN, as a result of the increased conductivity and surface area derived from carbon black support.[12] To further clarify the role of substrates, ordered porous carbon materials, such as CMK-3, were then adopted as their morphology and structures were easy to control.[11] It was shown incorporation of GCN into CMK-3 led to a direct $4e^-$ pathway, in consistent with

the theoretical prediction.[11] However, the small mesopores in CMK-3 may not be capable of fast mass exchange during ORR and the catalytic activity of GCN@CMK-3 was thus worse than that of the commercial Pt/C. From this point of view, uniform GCN embedded porous carbon (GCN/C) composites with tuneable pore size have been prepared.[13] The ORR activity of macroporous GCN/C with pore size of 150 nm was shown superior to that of the mesoporous GCN/C with pore size of 12 nm obtained via the similar synthesis route. The macroporous GCN/C facilitated the oxygen diffusion, and led to a much smaller Tafel slope value in the high overpotential region than that of the mesoporous sample. However the overall electron transfer number for this macroporous composite was only three, indicating a combined $2e^-$ and $4e^-$ reaction pathway, which was probably due to the low specific surface area and the lack of exposed active sites.[13] So far, none of the aforementioned carbon-supported GCN composites can show both fast ORR kinetics and excellent selectivity of $4e^-$ catalysis pathway.

Compared with carbon-based supports, 2D graphene sheets (GS) are expected to be a better substrate, given the excellent electron collection and transport properties of GS and its structural similarity to GCN.[6b,14] One latest theoretical investigation demonstrated that the π-π interaction at the interface of hybrid GS/GCN composites could force electrons to transfer from GS to GCN and accumulate on the active sites in GCN, which was predicted to significantly enhance the ORR catalytic activity.[15] However the early investigation of immobilizing GCN on GS only showed limited improvement – the ORR occurred via a $3e^-$ pathway with reduction current density slightly lower than that of the home-made platinum-loaded graphene composite.[10] Such an improvement was below expectation because only the effect of conductivity was considered and the GCN loading ratio (amount of active materials) was low (ca. 10 wt% nitrogen). In addition, the layered morphology was unfavorable for ORR due to the limited active sites exposure and the inefficient mass transport and access.[10] Inspired by that, here for the first time, we experimentally synthesized GS/GCN intercalated composites with hierarchical porosity. The ORR activity was first optimised by balancing two intrinsic parameters – active sites and conductivity. After further taking into account of mass transport, the obtained hierarchically porous GS/GCN intercalated composites showed fast reduction kinetics and 100% ORR catalysis selectivity, with better long-term stability and stronger tolerance against methanol than the commercial Pt/C catalysts. To the best of our knowledge, such excellent catalytic activities outperformed any other existing GCN-based ORR catalysts.[10-13,16]

Experimental Details

Synthesis of GO: Graphite oxide (GO) was synthesized by a modified Hummer method, as previously reported.[17] In a typical experiment, 5 g graphite (< 20 micron, Sigma-Aldrich) was vigorously stirred with 115 ml concentrated sulfuric acid (95-97%, Merck KGaA) in an ice bath (0 ^oC) and 15 g potassium permanganate (99+%, Sigma-Aldrich) was slowly added in to prevent a rapid temperature increase. The mixture was stirred in the ice bath for 30 minutes. After that the mixture was moved to an oil bath (30 ^oC) and was further stirred for 2 hours. Then 115 ml DI water (18.2 MΩ, Barnstead Easypure RoDi) was slowly added in and the temperature of the mixture may rise to ~40-45 ^oC. The diluted mixture was kept stirring at that temperature for another 30 minutes. Subsequently 700 ml DI water was added into the mixture followed by 50 ml hydrogen peroxide aqueous solution (30 wt%, Sigma-Aldrich). The mixture was left overnight before being washed with 6-7 L DI water with centrifuge (Heraeus Biofuge Primo). When the PH value of the drained water was 7, the obtained GO was freeze-dried (Virtis BT2KES) for about a week before further use.

Synthesis of GCN: GCN was synthesized by the polymerization of cyanamide, as previously reported.[18] In a typical experiment, cyanamide powder (99%, Sigma-Aldrich) was directly heated at 550 ^oC for 4 hours under nitrogen, with a ramping of 2.2 ^oC/min.

Synthesis of GSGCN: The GS/GCN intercalated composites were synthesized by wet chemical mixing of GO and cyanamide (GCN precursor) followed by thermal annealing. In a typical experiment, desirable mass ratios of cyanamide aqueous solution (50 wt%, Sigma-Aldrich) were added in 100 ml GO suspension (1 mg/ml). The mixture was sonicated for 1 hour till no visible precipitate. After that, the sample was dried in a vacuum oven (80 ^oC) overnight. The obtained grey/black powder was then grinded and transferred into a crucible with lid. For thermal annealing, the heating programme was the same as that for the synthesis of GCN – the sample was annealed 550 ^oC at 4 hours in nitrogen, with a ramping of 2.2 ^oC/min. The GS/GCN composites were labelled based on the mass ratio of cyanamide and GO, i.e. if 200 mg cyanamide was mixed with 100 mg GO, the obtained GS/GCN composite was marked as GSGCN_2x.

Synthesis of hp-GSGCN_2x: Similar to the synthesis of GSGCN_2x, but an extra 5 ml colloidal silica (40 wt% suspension in water, Sigma-Aldrich) was added to the mixture of cyanamide and GO before sonication. After heating at 550 ^oC, the obtained material was washed with 10 g ammonium bifluoride (95%, Sigma-Aldrich) for 24 hours, followed by filtration and washing with 1L DI water and 0.5 L ethanol (100%, Merck KGaA). The obtained hp-GSGCN_2x was dried in vacuum oven (80^oC) overnight before characterization.

Electrochemical Measurement: The cyclic voltammetry, rotating voltammetry and Chronoamperometric responses were measured in O_2-saturated 0.1M KOH. For electrode preparation, 4 mg catalyst was added in a mixture of 100 μl nafion (5 wt% in alcohol and water, Sigma-Aldrich) and 900 μl DI water, followed by one-hour sonication so as to well disperse sample in solvent. 5 μl catalyst suspensions were then drop casted on glassy carbon (GC) working electrode (3mm diameter, Metrohm) and dried at 60 ^oC. The ORR activity was tested in a three-electrode configuration. Ag/AgCl (sat. KCl, Sigma-Aldrich) was used as reference electrode and platinum sheet (Metrohm) was used as counter electrode. Oxygen was purged into electrolyte for an hour before measurement and kept bubbling during the tests, in order to make the electrolyte oxygen saturated. The scan rate for cyclic and rotating voltammetry was 100 and 10 mV/s respectively. Chronoamperometric responses for both methanol tolerance and long-term durability were measured at -0.3 V vs. Ag/AgCl. All the results were recorded by Metrohm Autolab 302N.

Characterization: The morphology and microstructure of the samples were investigated by scanning electron microscope

(JSM6301F, Japan), transmission electron microscopy (JEOL 2100, Japan) and X-ray diffraction (STOE Stadi P). Nitrogen sorption isotherms and BET surface areas were measured at 77 K with Quantachrome Autosorb iQ-c. The chemical composition was analyzed by Fourier transform infrared spectroscopy (Thermo Scientific Nicolet iS10), X-ray photon spectroscopy (Thermo Scientific K-Alpha, UK), and thermogravimetric analysis (Setaram Setsys 16/18). Electric conductivity was measured by the four-probe technique (Jandel RM3) with the pressed pellet of materials as samples. Typically, 200 mg sample was pressed by 10 tonnes for 5 minutes to form the pellet.

Results and Discussion

It is first shown under scanning electron microscope (SEM) that all GS/GCN composites possess a layered structure (Figures 1a and S1), similar to the morphology of GCN (Figure 1b) and GS (Figure 1c). The X-ray diffraction (XRD) patterns display that the peak positions of the GS/GCN composites are at 26.9°, corresponding to an interlayer distance of 3.31 Å, which can be further confirmed from the high-resolution transmission electron microscopy image (HRTEM, Figure 1d). The interlayer distances for GS and GCN are 3.27 and 3.44 Å, according to the peak positions at 25.9° and 27.3° respectively (Figure 1e). Note that the XRD peak positions of GS/GCN composites are between those of GS and GCN (highlighted by the dash lines in Figure 1e). Hence, the change in the interlayer distance suggests successful intercalation of GS into GCN layers.[10] The Brunauer-Emmett-Teller specific surface area (BET SSA) of GS/GCN composites (Figure 1f) derived from the nitrogen isotherm at 77 K (Figure S2) are within the range of 50-75 m^2/g, with a slight rise from GSGCN_1x to GSGCN_1.5x then drop as the GCN content in the composites further increases. The SSA of the intercalated GS/GCN composites is lower than the previously reported value for graphene-based materials[19] due to the restacking of graphene sheets during the formation of intercalated layered structures.

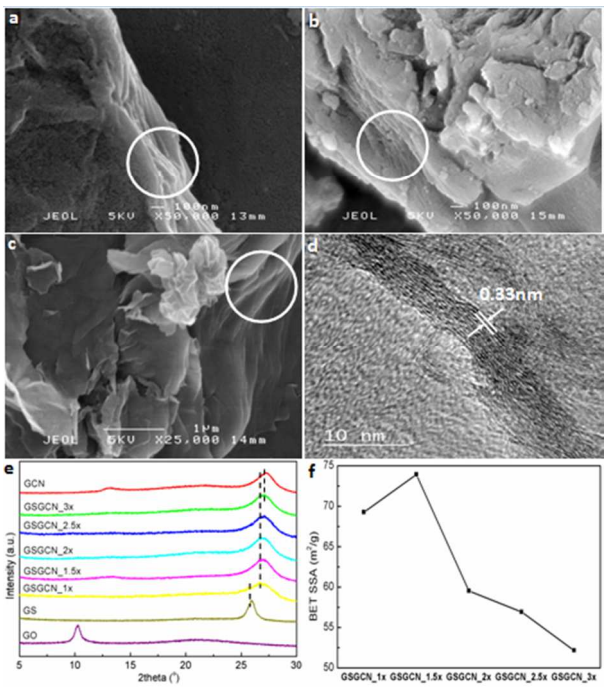

Fig 1. (a-c) SEM images of GSGCN_2x, GCN and GS. The layered morphology of GSGCN_2x, GCN and GS are highlighted by the white circles in the SEM images; (d) HRTEM image of GSGCN_2x; (e) XRD of GO, GS, GCN and GS/GCN composites. Those three dash lines exhibit the difference in the peak positions of GS, GCN and GS/GCN composites; and (f) BET SSA of GS, GCN and GS/GCN composites.

Chemical constitutions of the intercalated GS/GCN composites are then examined by the Fourier transform infrared spectroscopy (FTIR). Results (Figure 2) show that the out-of-plane bending vibration characteristics of heptazine rings[20] (~800 cm^{-1}, highlighted by the ellipse) for GCN are preserved in all GS/GCN composites, while the typical stretching vibration modes of heptazine-derived repeating units[20] (~1200-1650 cm^{-1}, highlighted by the straight lines in the inserted small plot) appear in GSGCN_2x, GSGCN_2.5x and GSGCN_3x but are not evident in GSGCN_1x and GSGCN_1.5x, implying either an incomplete polymerization or partial decomposition of GCN component for the latter two composites.[20c] What's more, it is noticed that GO has been successfully reduced to GS via thermal annealing as the non-sp2 carbon bonds (i.e. C-O, C=O and O-C=O) of GO significantly diminish in all GS/GCN composites[21] (highlighted by the straight lines in the main plot), which could be further supported by the X-ray photoelectron spectroscopy (XPS) results.

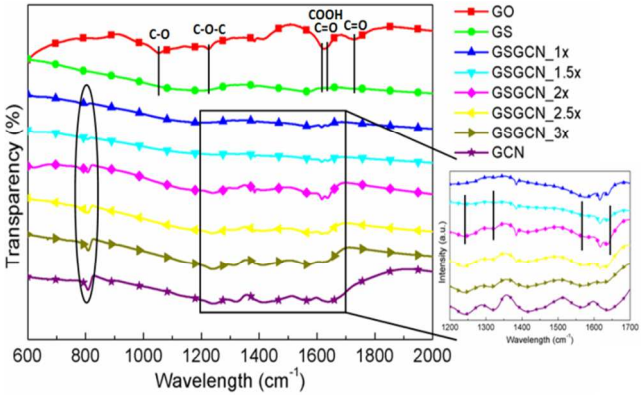

Fig 2. FTIR of GO, GS, GCN and GS/GCN composites. The ellipse and box (and also the lines in the inserted plot) represent the stretching mode of GCN; those lines in the main plot represent the vibration modes of epoxides, hydroxyls, carboxyls and ketones, respectively.

It is shown in XPS C1s spectra (Figure 3a) that the intensities of C-O bond (~286.5 eV) and C=O bond (~288 eV) are largely reduced in GS and GS/GCN composites and the atomic ratio of C_{sp2}/C_{sp3} increases from 0.9 for GO to 2.7 for GS.[22] Also the N-C=N bond (~288.3 eV) from GCN[22] could hardly been observed in GSGCN_1x and GSGCN_1.5x, in line with the FTIR results. It's worth noting that the C-C bond (~284.7 eV in GS/GCN)[22] and N-C=N bond (~288.1 eV in GS/GCN, if applicable) of GS/GCN composites show a right/left shift of ca. 0.1 eV compared with that of the pure GS and GCN respectively (highlighted by the dash lines in Figure 3a), which should be attributed to the strong electron transfer between the intercalated GS/GCN interfaces.[14] The relative ratios of pyridinic nitrogen bonding (~399 eV)[22d] derived from XPS N1s spectra for the GSGCN_1x and GSGCN_1.5x are much lower than that of pure

GCN (Figure 3b), confirming the incomplete polymerization or partial decomposition of GCN discovered in the FTIR.

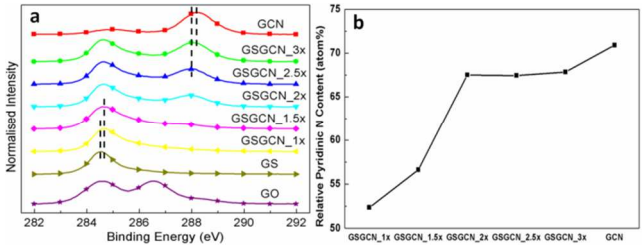

Fig 3. (a) XPS C1s spectra for GO, GS, GCN and GS/GCN composites; (b) the relative pyridinic nitrogen content in GCN and GS/GCN.

The residual mass of the GS/GCN composites after thermogravimetric (TG) analysis (Figure 4a) could be used to estimate the mixing ratio of GS/GCN in the composites[23] since GCN has almost completely decomposed after heating at 800 °C while no significant weight change could be detected for GS. The decrease of the GS content in the composites, from GSGCN_1x to GSGCN_3x, is in agreement with the increasing nitrogen content derived from the XPS (Figure 4b). Note that the intercalation of GCN into GS layer lowers the GCN decomposition temperature of ca. 30 °C (Figure 4a), indicating this intercalated hybrid structure decreases the decomposition temperature of GCN. Hence the lack of GCN pattern in GSGCN_1x and GSGCN_1.5x should be attributed to the partial decomposition of GCN.

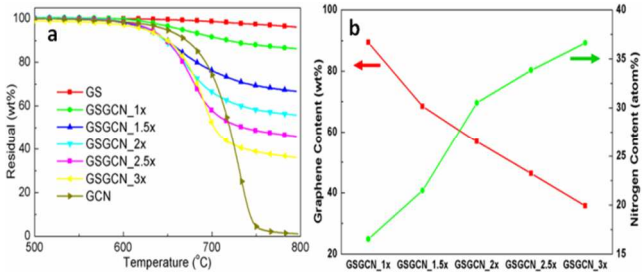

Fig 4. (a) TG patterns for GS, GCN and GS/GCN composites; (b) GS content in GS/GCN composites derived from the TG results and nitrogen content derived from XPS.

The electrocatalytic behaviors of intercalated GS/GCN composites are examined by cyclic voltammetry (CV) and the current density presented here equals the measured current divided by the geometric surface area of GC electrode. As shown in Figure 5 that the ORR performances of all the GS/GCN composites with different GCN ratios are superior to that of pure GCN, in terms of both onset/peak reduction potential and current density. More importantly, as the GCN content in the composites increases initially, from GSGCN_1x to GSGCN_2x, the reduction current density increases while the onset/peak reduction potential remains the same; but when GCN content further increases, from GSGCN_2x to GSGCN_3x, both the reduction current density and potential decrease considerably and gradually show a pattern similar to that of pure GCN. Such phenomena could also be confirmed by linear sweep voltammetry (LSV) measurement (Figure S3).

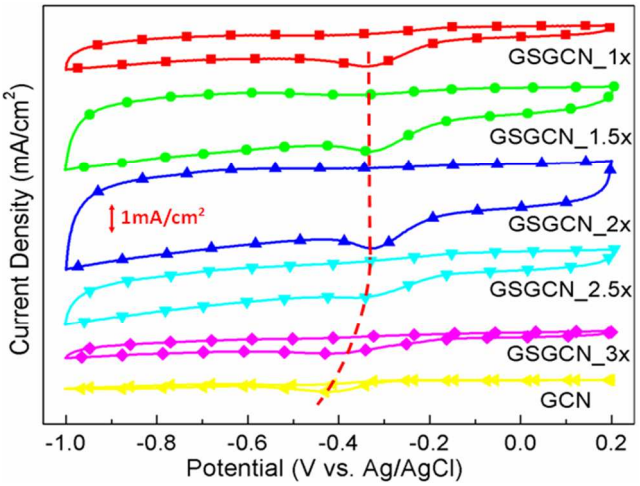

Fig 5. CV of GS/GCN composites and GCN in 0.1M KOH (scan rate 100mv/s). The red curve highlights the shift of peak reduction potential for GS/GCN composites.

To explain the above observations on the ORR properties of GS/GCN intercalated composites, both structural characteristics and chemical composition need to be considered. Particularly the BET SSA (m^2/g) and total nitrogen content from XPS (atom%) should be taken into account, as the surface nitrogen heteroatom is the origin of ORR catalytic activity.[6a] Here we introduce a new parameter called 'effective-SSA' (E-SSA), which is defined as the product of SSA and nitrogen content. In this sense, E-SSA could represent the amount of active sites, and E-SSA normalized peak reduction current thus represents the conductivity, assuming no major difference in the mass transport capability for GS/GCN composites as they all possess layered structures, the similar macro-morphology. It is shown in Figure 6, when the GCN content in the composites is low, the E-SSA normalized current is almost a constant, indicating sufficient conductivity supplied by the intercalated GS. As a result, the ORR performances, similar reduction potential but increasing current density from GSGCN_1x to GSGCN_2x, are dependent on the amount of active sites. However when the GCN content is in excess, though the E-SSA of GSGCN_2.5x and GSGCN_3x is similar to that of GSGCN_2x, the E-SSA normalized current decreases significantly, in accordance with the rapid decline in both reduction potential and peak current density. This suggests the amount of GS in the composites no longer affords to provide enough conductivity and the ORR activity turns into conductivity dependent. Accordingly, GSGCN_2x shows the best ORR performance among all five GS/GCN intercalated composites because it possesses the largest amount of active sites while remains sufficient conductivity. The increase in electrical conductivity, which is led by the intercalation of GS into GCN layers, is one of the key requirements for the improved ORR activities. Such an enhancement can be confirmed by the four-probe conductivity measurement (Table S1). Typically, the powder conductivity for GCN is under the detection limitation of the instrument, and thus must be smaller than 10^{-2} S/cm, similar to the previous report.[10] For GS/GCN intercalated composites, the conductivity is about 0.5-4.5 S/cm, i.e. 3.06 S/cm for GSGCN_2x, at least two magnitudes greater than that of pristine GCN.

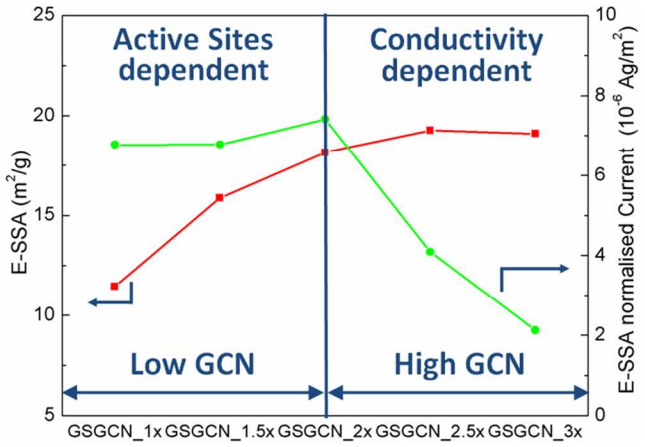

Fig 6. E-SSA and E-SSA normalized peak current for GS/GCN composites, calculated from the CV, BET and XPS nitrogen content.

Mass transport is another crucial factor for ORR besides active sites and electrical conductivity.[24] Though macropores are capable of fast oxygen exchange during ORR, the relatively low surface area leads to a lack of exposed active sites.[13,25] It is thus expected hierarchical porosity with combined macropores and mesopores may solve the dilemma of both high accessibility and high surface area, as macropores can promise efficient mass transport while mesopores offer sufficient accessible active sites. Here we demonstrate such a hierarchically porous GS/GCN intercalated composite (hp-GSGCN_2x) can be easily fabricated by the addition of excess silica nanospheres before the polymerization of GCN. The macroporosity of the obtained hp-GSGCN_2x is confirmed by SEM (Figure 7a) and the mesopores with an average size close to the diameter of individual silica sphere template (ca. 10 nm) are shown under HRTEM (Figure 7B). Note that the interlayer spacing of hp-GSGCN_2x (~0.33 nm, as shown in HRTEM) is close to that of GSGCN_2x, which means the hp-GSGCN_2x also remains the intercalated structure. The XPS patterns of hp-GSGCN_2x are similar to those of GSGCN_2x with a slight decrease in nitrogen content, but the SSA of hp-GSGCN_2x is ~50% greater than that GSGCN_2x (Figure S2), giving the overall E-SSA roughly 30% higher.

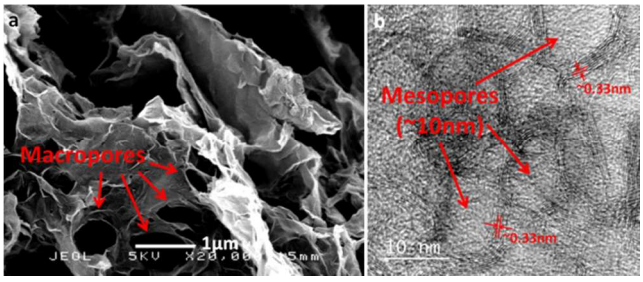

Fig 7. (a) SEM and (b) HRTEM of hp-GSGCN_2x.

The ORR activities of hp-GSGCN_2x are first assessed by CV. As shown in Figure 8a, the peak current density of hp-GSGCN_2x is almost 1.5 times higher than that of GSGCN_2x and the onset/peak reduction potential also increases by ~30 mV, which is further confirmed by LSV (Figure 8b and S4). Surprisingly, though the onset reduction potential of hp-GSGCN_2x is still lower than that of Pt/C, the current density surpasses Pt/C at a potential of only -0.24 V vs. Ag/AgCl and the half wave potential is only 90 mV lower. The electron transfer numbers for GSGCN_2x and hp-GSGCN_2x are calculated by the Koutecky-Levich equation:[3a]

$$1/J = 1/J_L + 1/J_K = 1/0.62nFC_0(D_0)^{2/3}v^{-1/6}\omega^{1/2} + 1/J_K$$

where J is the measured current density (mA/cm^2), J_L and J_K are the diffusion-limiting and kinetic current densities (mA/cm^2) respectively, n is the overall number of electron transferred in the oxygen reduction, F is Faraday constant (96483 sA/mol), C_0 is the bulk saturated concentration of O_2 in 0.1 M KOH (1.2×10^{-3} mol/L), D_0 is the diffusion coefficient of O_2 in 0.1 M KOH (1.9×10^{-5} mol/L), ν is the kinematic viscosity of the 0.1 M KOH (0.01 m^2/s), and ω is angular velocity of the disk (rad/s). According to the Koutecky-Levich plots (K-L plots, 1/J vs. $\omega^{1/2}$, Figure 8c), the number of electron exchanged during ORR can be calculated from the slope, $1/0.62nFC_0(D_0)^{2/3}v^{-1/6}$.[3a] It is seen from Figure 8c that the K-L plot of h-GSGCN_2x at -0.4 V vs. Ag/AgCl is parallel to the straight line for theoretical 4e$^-$ pathway, and the electron transfer number is calculated to be 3.98 (Figure 8d);[3] on the other hand, the electron transfer number for GSGCN_2x is only 2.25, close to an indirect 2e$^-$ pathway. In addition, the efficient 4e$^-$ transfer for hp-GSGCN_2x can also observed within a broad potential range from -0.3 to -0.6 V vs. Ag/AgCl, as shown in the Figure 8d. Such excellent catalysis selectivity and fast ORR kinetics at a relatively high potential region should be attributed to the synergistic effect of the balanced active sites and electrical conductivity and so as the pre-designed hierarchically porous structure, especially those macrospores for facile mass transport. The enhancement in ORR performance derived from the hierarchical porosity can be further confirmed by the significantly reduced Tafel slope at the high potential range of -0.15 to -0.2 V vs. Ag/AgCl (70.6 and 108.9 mV/dec for hp-GSGCN_2x and GSGCN_2x respectively, Figure S5).[13] As far as we know, none of the existing metal-free GCN-based ORR catalysts possesses both the aforementioned excellent catalysis selectivity and fast ORR kinetics at such a relatively high potential region (Table S2). However, it is also noted that although the catalytic activity of the hp-GSGCN_2x has been dramatically improved, it still can't compete with the commercial Pt/C, particularly in terms of the onset/half-wave reduction potential. Considering the overall energy efficiency of metal-air batteries highly depends on the over-potential, our continuous effort is to introduce other non-precious metal based catalysts with higher onset reduction potential (i.e. iron or cobalt based) into the current hierarchically porous GS/GCN intercalated composites. It is expected the strong interaction between the obtained metal/metal oxide and nitrogen-doped carbon, as well as the synergistic effect of two different active sites, can lead to much higher onset/peak reduction potential while retaining the excellent catalysis selectivity and fast kinetics.

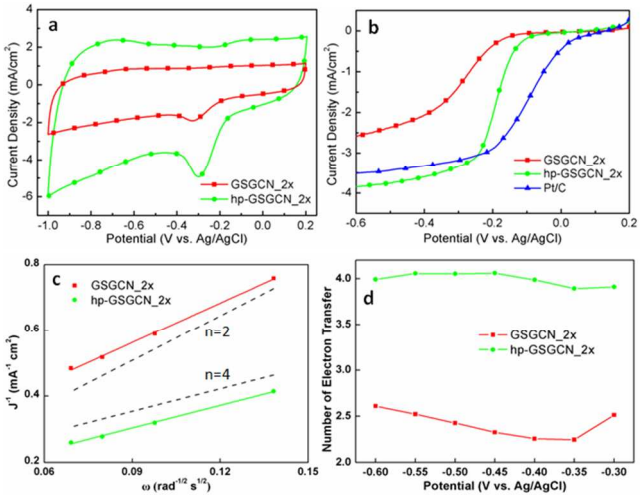

Fig 8. (a) CV of GSGCN_2x and hp-GSGCN_2x (scan rate: 100 mV/s); (b) LSV of GSGCN_2x, hp-GSGCN_2x and Pt/C at 1500 rpm (scan rate: 10 mV/s); (c) K-L plots of GSGCN_2x and hp-GSGCN_2x at -0.4 V (dashed lines represent the K-L plots for the theoretical $2e^-$ and $4e^-$ pathway); (d) number of electron transfer for GSGCN_2x and hp-GSGCN_2x at -0.3 to -0.6 V.

Since safety is the first priority to the widespread application of electric vehicles,[26] the tolerance against the methanol crossover effect should be of particular importance to the direct methanol fuel cells (DMFC), and so as the long-term durability. The methanol tolerance is evaluated by the current-time response at -0.3 V vs. Ag/AgCl. Oxygen is purged into the electrolyte from 500 s and 3M methanol is added in after 3500 s. It is shown in Figure 9a that the ORR of Pt/C switches to a methanol oxidation reaction (MOR) after the addition of 3M methanol, as indicated by the shift to a positive current density;[3b] however the ORR activity of hp-GSGCN_2x is almost unaffected. The long-term durability of hp-GSGCN_2x and commercial Pt/C is also assessed through the chronoamperometric response at -0.3 V vs. Ag/AgCl. The ten-hour test only causes a slight activity loss for hp-GSGCN_2x, whereas Pt/C loses nearly 40% of its initial activity. These two measurements confirm that the hp-GSGCN_2x in this work is much more stable in the alkaline electrolyte and against the methanol cross-over effect, compared with the commercial Pt/C.

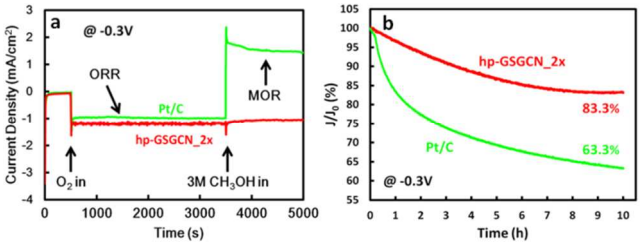

Fig 9. Chronoamperometric response of hp-GSGCN_2x and Pt/C at -0.3 V vs. Ag/AgCl for (a) tolerance against methanol and (b) long-term stability.

Conclusions

In this work, a facile synthesis method of hierarchically porous GS/GCN intercalated composites is presented, which display much better ORR activities than the existing GCN-based catalysts and also improved durability and methanol tolerance compared with commercial Pt/C. Firstly, the electrochemical properties of GS/GCN intercalated composites without hierarchical porosity are optimised, by changing the mixing ratio of GS/GCN to balance the amount of active sites and electrical conductivity. Based on that, a hierarchically macro/mesoporous structure is designed, so as to achieve both efficient mass transport and sufficient exposed active sites. The obtained hp-GSGCN_2x shows the smaller half wave potential difference with commercial Pt/C than any other GCN-based ORR catalysts, and so as the highest potential when current density outperforms Pt/C. In addition, it possesses 100% $4e^-$ catalysis pathway selectivity within a broad potential region of -0.3 to -0.6 V vs. Ag/AgCl. The long-term stability and tolerance to methanol crossover effect is also significantly improved, compared with the commercial Pt/C. In this regard, it is reasonable to anticipate that such a hierarchically porous GS/GCN intercalated composite could be a promising future catalyst for both fuel cells and metal-air batteries.

Acknowledgement

This work is supported by Engineering and Physical Sciences Research Council (EPSRC) grant (Ref: EP/K002252/1).

Notes and references

[a] *Department of Chemistry, University College London, 20 Gordon Street, London, WC1H 0AJ, UK. Tel: 07869738380; E-mail: k.qiu.12@ucl.ac.uk*

† Electronic Supplementary Information (ESI) available. See DOI: 10.1039/b000000x/

1 1 (a) B. C. Steele and A. Heinzel, *Nature*, 2001, **414**, 345; (b) F. Cheng and J. Chen, *Chem. Soc. Rev.*, 2012, **41**, 2172.

2 (a) M. Winter and R. J. Brodd, *Chem. Rev.*, 2004, **104**, 4245; (b) X Yu and S. Ye, *J. Power Source*, 2007, **172**, 133; (c) B. Lim, M. J. Jiang, P. H. C. Camargo, E. C. Cho, J. Tao, X. M. Lu, Y. M. Zhu and Y. N. Xia, *Science*, 2009, **324**, 1302.

3 (a) R. Liu, D. Wu, X. Feng and K. Müllen, *Angew. Chem. Int. Ed.*, 2010, **49**, 2565; (b) W. Yang, T. P. Fellinger, and M. Antonietti, *J. Am. Chem. Soc.*, 2010, **133**, 206.

4 J. Greeley, I. E. L. Stephens, A. S. Bondarenko, T. P. Johansson, H. A. Hansen, T. F. Jaramillo, J. Rossmeisl, I. Chorkendorff and J. K. Norskov, *Nature Chem.*, 2009, **1**, 552.

5 M. Lefevre, E. Proietti, F. Jaouen, and J. P. Dodelet, *Science*, 2009, **324**, 71.

6 (a) K. Gong, F. Du, Z. Xia, M. Durstock and L. Dai, *Science*, 2009, **323**, 760; (b) Y. Zheng, Y. Jiao, M. Jaroniec, Y. Jin and S. Z. Qiao, *Small*, 2012, **8**, 3550; (c) L. Yang, S. Jiang, Y. Zhao, L. Zhu, S. Chen, X. Wang, Q. Wu, J. Ma, Y. Ma, and Z. Hu, *Angew. Chem. Int. Ed.*, 2011, **50**, 7132; (d) Y. Zhao, L. Yang, S. Chen, X. Wang, Y. Ma, Q. Wu, Y. Jiang, W. Qian and Z. Hu, *J. Am. Chem. Soc.*, 2013, **135**, 1201.

7 (a) S. F. Huang, K. Terakura, T. Ozaki, T. Ikeda, M. Boero, M. Oshima, J. I. Ozaki and S. Miyata, *Phys. Rev. B*, 2009, **80**, 235410; (b) X. Hu, Y. Wu, H. Li, and Z. Zhang, *J. Phys. Chem. C*, 2010, **114**, 9603; (c) L. Zhang and Z. Xia, *J. Phys. Chem. C*, 2011, **115**, 11170.

8 (a) S. Yang, X. Feng, X.Wang, and K. Müllen, *Angew. Chem. Int. Ed.*, 2011, **50**, 5339; (b) S. Chen, J. Bi, Y. Zhao, L. Yang, C. Zhang, Y. Ma, Q. Wu, X. Wang and Z. Hu, *Adv. Mater.*, 2012, **24**, 5593; (c) T. Sharifi, G. Hu, X. Jia, and T. Wagberg, *ACS Nano*, 2012, **6**, 8904; (d) L. Lai, J. R. Potts, D. Zhan, L. Wang, C. K. Poh, C. Tang, H. Gong, Z. Shen, J. Lin and R. S. Ruoff, *Energy Environ. Sci.*, 2012, **5**, 7936.

9 (a) A. Thomas, A. Fischer, F. Goettmann, M. Antonietti, J. O. Müller, R. Schlögl and J. M. Carlsson, *J. Mater. Chem.*, 2008, **18**, 4893; (b) P. Niu, L. Zhang, G. Liu, and H. M. Cheng, *Adv. Funct. Mater.*, 2012, **22**, 4763; (c) Y. Zheng, J. Liu, J. Liang, M. Jaroniec and S. Z. Qiao, *Energy Environ. Sci.*, 2012, **5**, 6717.

10 Y. Sun, C. Li, Y. Xu, H. Bai, Z. Yao and G. Shi, *Chem. Commun.*, 2010, **46**, 4740.

11 Y. Zheng, Y. Jiao, J. Chen, J. Liu, J. Liang, A. Du, W. Zhang, Z. Zhu, S. C. Smith, M. Jaroniec, G. Q. Lu and S. Z. Qiao, *J. Am. Chem. Soc.*, 2011, **133**, 20116.

12 S. M. Lyth, Y. Nabae, S. Moriya, S. Kuroki, M. A. Kakimoto, J. I. Ozaki and S. Miyata, *J. Phys. Chem. C*, 2009, **113**, 20148.

13 J. Liang, Y. Zheng, J. Chen, J. Liu, D. Hulicova-Jurcakova, M. Jaroniec and S. Z. Qiao, *Angew. Chem. Int. Ed.*, 2012, **51**, 3892.

14 S. Pei and H. M. Cheng, *Carbon*, 2012, **50**, 3210.

15 A. Du, S. Sanvito, Z. Li, D. Wang, Y. Jiao, T. Liao, Q. Sun, Y. H. Ng, Z. Zhu, R. Amal and S. C. Smith, *J. Am. Chem. Soc.*, 2012, **134**, 4393.

16 K. Kwon, Y. J. Sa, J. Y. Cheon, and S. H. Joo, *Langmuir*, 2012, **28**, 991.

17 J. W. Burress, S. Gadipelli, J. Ford, J. M. Simmons, W. Zhou and T. Yildirim, *Angew. Chem. Int. Ed.*, 2010, **49**, 8902.

18 X. Wang, K. Maeda, A. Thomas, K. Takanabe, G. Xin, J. M. Carlsson, K. Domen and M. Antonietti, *Nature Mater.*, 2009, **8**, 76.

19 (a) M. D. Stoller, S. J. Park, Y. W. Zhu, J. H. An and R. S. Ruoff, *Nano Lett.*, 2008, **8**, 3498; (b) Y. Zhu, S. Murali, M. D. Stoller, A. Velamakanni, R. D. Piner and R. S. Ruoff, *Carbon*, 2010, **48**, 2118; (c) S. R. C. Vivekchand, C. S. Rout, K. S. Subrahmanyam, A. Govindaraj and C. N. R. Rao, *J. Chem. Sci.*, 2008, **120**, 9.

20 (a) M. J. Bojdys, J. O. Müller, M. Antonietti and A. Thomas, *Chem. Eur. J.*, 2008, **14**, 8177; (b) S. C. Yan, Z. S. Li and Z. G. Zou, *Langmuir*, 2009, **25**, 10397; (c) F. Dong, L. Wu, Y. Sun, M. Fu, Z. Wu and S. C. Lee, *J. Mater. Chem.*, 2011, **21**, 15171; (d) J. Liu, T. Zhang, Z. Wang, G. Dawsona and W. Chen, *J. Mater. Chem.*, 2011, **21**, 14398.

21 Y. Zhang, T. Mori, L. Niu and J. Ye, *Energy Environ. Sci.*, 2011, **4**, 4517.

22 (a) X. Li, H. Wang, J. T. Robinson, H. Sanchez, G. Diankov and H. Dai, *J. Am. Chem. Soc.*, 2009, **131**, 15939; (b) C. Zhang, L. Fu, N Liu, M. Liu, Y. Wang and Z. Liu, *Adv. Mater.*, 2011, **23**, 1020; (c) Z. Sheng, L. Shao, J. Chen, W. Bao, F. Wang and X. Xia, *ACS Nano*, 2011, **5**, 4350; (d) H. Wang, T. Maiyalagan and X. Wang, *ACS Catal.*, 2012, **2**, 781.

23 (a) Y. Zhang, T. Mori, Li Niu and J. Ye, *Energy Environ. Sci.*, 2011, **4**, 4517; (b) X. Li, J Chen, X. Wang, J. Sun and M. Antonietti, *J. Am. Chem. Soc.*, 2011, **133**, 8074.

24 (a) M. Mirzaeian and P. J. Hall, *Electrochim. Acta*, 2009, **54**, 7444; (b) G. O. Shitta-Bey, M. Mirzaeian, and P. J. Hall, *J. Electrochem. Soc.*, 2012, **159**, A315.

25 J. Liang , X. Du , C. Gibson , X.Du and S. Z. Qiao, *Adv. Mater.*, 2013. DOI: 10.1002/adma.201302569

26 (a) J. B. Goodenough and Y. Kim, *Chem. Mater.*, 2010, **22**, 587; (b) M. Mirzaeian and P. J. Hall, *J. Power Source*, 2010, **195**, 6817.

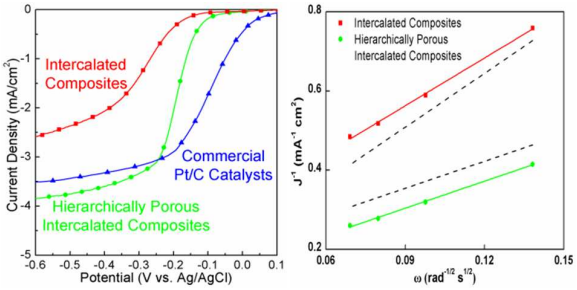

The hierarchically porous graphene sheets / graphitic carbon nitride intercalated composites are promising alternatives to platinum-based oxygen reduction catalysts.